SCIENCE CHINA
Earth Sciences

•RESEARCH PAPER•

September 2020 Vol.63 No.9: 1390–1407
https://doi.org/10.1007/s11430-019-9606-4

Annual 30-m land use/land cover maps of China for 1980–2015 from the integration of AVHRR, MODIS and Landsat data using the BFAST algorithm

Yidi XU[1], Le YU[1,2*], Dailiang PENG[3], Jiyao ZHAO[1], Yuqi CHENG[1], Xiaoxuan LIU[1], Wei LI[1], Ran MENG[4], Xinliang XU[5] & Peng GONG[1,2]

[1] *Ministry of Education Key Laboratory for Earth System Modeling, Department of Earth System Science, Tsinghua University, Beijing 100084, China;*
[2] *Ministry of Education Ecological Field Station for East Asian Migratory Birds, Beijing 100084, China;*
[3] *Key Laboratory of Digital Earth Science, Institute of Remote Sensing and Digital Earth, Chinese Academy of Sciences, Beijing 100094, China;*
[4] *College of Natural Resources and Environment, Huazhong Agricultural University, Wuhan 430070, China;*
[5] *State Key Laboratory of Resources and Environmental Information Systems, Institute of Geographical Sciences and Natural Resources Research, Chinese Academy of Sciences, Beijing 100101, China*

Received October 2, 2019; revised March 9, 2020; accepted March 21, 2020; published online May 19, 2020

Abstract Annual land use land cover (LULC) change information at medium spatial resolution (i.e. at 30 m) is required in numerous subjects, such as biophysical modelling, land management and global change studies. Annual LULC information, however, is usually not available at continental or national scale due to reasons such as insufficient remote sensing data coverage or lack of computational capabilities. Here we integrate high temporal resolution and coarse spatial resolution satellite images (i.e., Moderate Resolution Imaging Spectroradiometer (MODIS) and Global Inventory Modelling and Mapping Studies (GIMMS) normalized difference vegetation index (NDVI)) with high spatial resolution datasets (China's Land-Use/cover Datasets (CLUDs) derived from 30-meter Landsat TM/ETM+/OLI) to generate reliable annual nominal 30 m LULC maps for the whole of China between 1980 and 2015. We also test the performance of a statistical based change detection algorithm (Breaks for Additive Seasonal and Trend), originally designed for tracking forest change, in classifying all-type LULC change. As a result, a nominal 30 m annual land use/land cover datasets (CLUD-A) from 1980 to 2015 was developed for the whole China. The mapping results were assessed with a change sample dataset, a regional annual validation sample set and a three-year China sample set. Of the detected change years, 75.61% matched the exact time of conversion within ±1 year. Annual mapping results provided a detail process of urbanization, deforestation, afforestation, water and cropland dynamics over the past 36 years. The consistent characterization of land change dynamics for China can be further used in scientific research and to support land management for policy-makers.

Keywords Land use land cover (LULC), Breaks for Additive Seasonal and Trend (BFAST), Change detection, Annual, China

Citation: Xu Y, Yu L, Peng D, Zhao J, Cheng Y, Liu X, Li W, Meng R, Xu X, Gong P. 2020. Annual 30-m land use/land cover maps of China for 1980–2015 from the integration of AVHRR, MODIS and Landsat data using the BFAST algorithm. Science China Earth Sciences, 63: 1390–1407, https://doi.org/10.1007/s11430-019-9606-4

* Corresponding author (email: leyu@tsinghua.edu.cn)

1. Introduction

China has undergone rapid growth in its population and economy over the past decades, which has transformed its land surface (Liu et al., 2005). To feed the world's largest population (1.36 billion in 7.06 billion globally), significant cropland expansion has occurred in the north-east and north-west regions, resulting in the loss of natural grassland, forest cover and water resources (Akiyama and Kawamura, 2007; Hu et al., 2015; Zhou et al., 2017). Urbanization, with rapid growth in the urban population and intensive human activities, has also played a role in land surface change in China (Schneider and Mertes, 2014). In recent decades, land restoration policies, such as the "Grain for Green" and "Three North Shelterbelt" projects, have reshaped land use practice in some ecologically vulnerable regions in China such as Inner-Mongolia (Ding, 2003; Yin et al., 2018). So far, reliable dynamic land cover change information in China including magnitude, extent, change trajectory and cause-effect relationships remains poorly documented (Lin and Ho, 2003), which hampers an in depth understanding of the land change trajectory and consequent land resources management.

Remote sensing provides an efficient, economical and consistent way to track land use/land cover (LULC) changes. So far, many global and national mapping programs have been launched to capture the long-term LULC dynamics (Cotillon, 2017; Feranec et al., 2016; Jin et al., 2017; Ngcofe and Thompson, 2015). Efforts have also been made in studying annual land cover changes at global scale such as Moderate Resolution Imaging Spectro-radiometer annual Land Cover product (MODIS-LC) at 500 m resolution (Friedl et al., 2002) and an annual 300 m global Land Cover products by European Space Agency Climate Change Initiative (ESA-CCI) (Defourny et al., 2017). Song et al. (2018) derived the longest global land cover datasets (1992–2016) using multiple optical observations. Recently, Liu et al. (2019) provided annual global LULC at 5 km resolution using the Global Land Surface Satellite (GLASS) Climate Data Records (CDRs). In the case of China, annual land use land cover changes were mapped at 8 km using Global Inventory Modelling and Mapping Studies (GIMMS) normalized difference vegetation index (NDVI) 3g data (He et al., 2017). However, these studies have all been conducted at coarse resolution (hundreds or thousands of meters) and have failed to meet the demands of land management (Yu et al., 2014; Zhong et al., 2014), particularly for regions like southern China which is dominated by smallholdings and intensive farming. Furthermore, great discrepancies have been found in heterogeneous landscapes when comparing the commonly used coarse LULC datasets (Bai et al., 2014; Gong et al., 2013; Liu et al., 2005). For example, one estimation of cropland area in China by Advanced Very High Resolution Radiometer (AVHRR) is 48% higher than the national census (Frolking et al., 1999). The complexity of land-cover areas and quick land use modifications calls for finer resolution LULC products in China (i.e., 30-m spatial resolution) (Lu et al., 2016). In recent decades, 30-m Landsat data have been widely used in forest, water and cropland mapping and monitoring (Gong et al., 2010; Hansen et al., 2013; Hu et al., 2014; Pekel et al., 2016; Yu et al., 2013, 2014). In China, some pilot studies explored the 30 m land change information at yearly frequency for certain type such as impervious surface (Gong et al., 2019; Li et al., 2015; Zhang et al., 2017) and paddy rice (Dong et al., 2015). But annual application to all-type land cover maps for the whole of China at 30-m resolution require further exploration.

China's Land-Use/cover Dataset (CLUD) at 30-m resolution for the 1980s, 1995, 2000, 2005, 2010 and 2015 using Landsat imagery provides unprecedented LULC detail for China (Liu et al., 2014; Ning et al., 2018). However, these datasets are interpreted by human operators and are difficult to apply at yearly scale because of the huge workload involved. To expand multi-decadal to annual LULC dynamics, two approaches have been commonly used: (1) time-series analysis, which has mainly focused on a single type of mapping (e.g., tracking the disturbance and recovery of forest or mapping the cultivation and abandonment of cropland) (Dong et al., 2015; Huang et al., 2010; Kennedy et al., 2010; Verbesselt et al., 2010b; Zhao et al., 2016), and (2) obtaining yearly LULC mapping and change information based on annual LULC classification results (Li et al., 2015; Xu et al., 2017). However, the former method, based on temporal profile analysis, lacks "from-to" information. These studies were mainly applied in a limited region with single type of land cover change, e.g., "forest disturbance and recovery". The latter method requires abundant Landsat images (>4) (Xu et al., 2018a) which were not available in most of the regions outside the United States before 1990. Annual classification may also lead to pseudo changes.

In the case of China, most regions in south-east and south-west China face the challenge of insufficient Landsat data for annual mapping and change detection (Figure S1, https://link.springer.com). A possible approach to address the data challenge is to combine multiple resolution satellite datasets (Yin et al., 2018) by fusing the coarse datasets with the finer ones (Gao et al., 2017; Kwan et al., 2018). However, data fusion aimed at bridging gaps cannot replace actual satellite missions (Gao et al., 2015). Here, we provide a new approach by combining CLUD (1980s, 1995, 2000, 2005, 2010 and 2015) with the Moderate Resolution Imaging Spectro-radiometer (MODIS) and AVHRR GIMMS datasets by a well-developed statistical boundary-based change detection algorithm known as Breaks for Additive Seasonal and Trend (BFAST), to track annual LULC changes over the past four decades (1980–2015). The production of annual land cover

dataset is based on a new and simple methodology: the six LULC maps in CLUD provide the change information for each period, and the final annual results can be updated by detecting the exact change year using the time-series coarse observations among each interval. BFAST has been widely used in detecting the change patterns in vegetation types (de Jong et al., 2012; Watts and Laffan, 2014), but the effectiveness in the shift among all LULC types has not been explored. The objectives of this study are threefold: (1) to develop a breakpoint-based long-term annual LULC mapping approach using coarse remote sensing datasets and high-resolution LULC datasets; (2) to evaluate the performance of the statistical based change detection algorithm, BFAST, in exploring all-type LULC changes; (3) to develop annual land use/land cover datasets (called CLUD-A) for China at nominal 30-m resolution.

2. Datasets and methods

2.1 Datasets

2.1.1 China's Land-Use/cover Datasets

CLUD at 30 m resolution for the 1980s, 1995, 2000, 2005, 2010 and 2015 were used as the base maps for developing nominal 30 m annual land use/land cover datasets CLUD-A from 1980 to 2015. The CLUD were generated from the Landsat Multispectral Scanner (MSS), Thematic Mapper (TM), Enhanced Thematic Mapper Plus (ETM+), and Operational Land Imager (OLI), combined with multispectral data from the Huanjing-1 satellite (HJ-1). After conducting pre-processing steps including image fusion, geometric correction, image enhancement and splicing, LULC maps were derived through human-computer interaction and visual interpretation. The datasets describe the land surface in six first-level categories (Cropland, Forest, Grassland, Water body, Built-up land, and Unused land) and 25 second-level categories. The unused land includes sand, Gobi, saline land, marshland, barren land and other land which is not used until the mapping time. Validation of the dataset was carried out using field surveys and the average classification accuracy of the six primary land cover classes reached 94.3%, while the mapping accuracy of the 25 sub-classes was above 91.2% (Liu et al., 2014, 2005, 2003; Ning et al., 2018). Here we assume that CLUD with above 91.2% reported accuracy can serve as reliable base maps in subsequent processes.

2.1.2 Satellite datasets

To fully cover the entire study period, we used multi-source remote sensing images including the MODIS and AVHRR to derive the CLUD-A. The NDVI derived from these sensors is a critical index for vegetation conditions, and has been widely used in monitoring forest disturbance and recovery, cropland phenology and other LULC change studies (Ding et al., 2016; Forkel et al., 2013; Lunetta et al., 2006). Here, Landsat imagery was not used because of the poor data availability in the early stages (i.e., 1980–1990) (see the blank path/rows in Figure S1). The spatial resolution of the MODIS data (250 m) and GIMMS data (8 km) is coarser than Landsat images (30 m) but these two datasets have a denser temporal resolution.

(1) MODIS dataset**.** MODIS NDVI 16-day composite grid data (MOD13Q1 collection 6, the recent updated version) from 2000 to 2015 were provided by NASA's Earth Observing System Data and Information System gateway (https://earthdata.nasa.gov/). The MOD13Q1 product consists of 1200 km×1200 km tiles of 250-m resolution, which is gridded in a sinusoidal projection. It was used as the main satellite data to conduct change detection within the interval years of CLUD after 2000 (2000–2005, 2005–2010 and 2010–2015). Poor-quality pixels covered by cloud were not used in the analysis. In total, 19 MODIS tiles were utilized to cover the whole China.

(2) GIMMS dataset**.** The second dataset used in this study for the period before 2000 was the AVHRR GIMMS NDVI dataset. The latest version, GIMMS NDVI 3g.v1 dataset provides the longest satellite temporal coverage from 1982 to 2015 at 8-km spatial resolution and can be used in land cover maps. This product is composited based on the maximum NDVI value for each pixel every 15 days (Holben, 1986). The dataset was corrected for problems such as calibration loss, orbital drift, and atmospheric effects such as volcanic eruptions.

2.2 Methods

The process of producing the CLUD-A includes (1) data preparation (both the CLUD and time-series NDVI datasets of MODIS and GIMMS) (Section 2.2.1), (2) change-detection analysis (Section 2.2.2) and (3) annual LULC mapping (Section 2.2.3). The validation of the LULC datasets is described in Section 2.2.4.

2.2.1 Data preparation

Given the time of the original maps from CLUD (1980, 1995, 2000, 2005, 2010 and 2015), subsequent analysis including the production of the change map, preparation of the time-series NDVI datasets, change-detection analysis and annual LULC updates were conducted in different time periods, P1: 1980–1995, P2: 1995–2000, P3: 2000–2005, P4: 2005–2010 and P5: 2010–2015. The CLUD, in six time phases, provide the land cover information for the start and end year of each period and the change areas for each period were derived based on the land cover maps from CLUD with spatial locations and "from-to" types. For example, given the land cover maps for 1980 and 1995 in CLUD, the change pixels were identified using these land cover maps (e.g.,

cropland (C) converted to built-up land (U) as shown in the top left corner of the magnified nine patch in Figure 1) while the unchanged pixels were masked in the change map from 1980 to 1995. As a result, five change maps for the five periods were derived for the change detection in the next step. Here, we considered the conversion between the six primary classes (e.g., conversions from grassland to water, forest to cropland) without the changes in the sub-classes (e.g., the conversions from rivers to lakes in the water class and desert to the Gobi in unused land) in this study. The conversion between sub-classes were not studied because of the lower classification accuracy in level 2 land-cover categories compared with lever 1 classes (Gong et al., 2013). The mapping process and an example for one period, 1980–1995, are shown in Figure 1a and 1b).

The pre-processing of the two NDVI datasets is indicated. We first re-projected all the MODIS imagery to a geographic grid with a WGS 1984 spheroid consistent with CLUD. Each coarser resolution dataset was resized to 30 m using the nearest neighbour resampling approach to match the CLUD following the previous practice (Feng et al., 2018). Several methods have been developed for the pre-processing of dense satellite datasets, including the image composition based on the thresholds (Hansen et al., 2013; Xu et al., 2018b), temporal metrics extraction (Waldner et al., 2015) and time-series trend analysis using all available data (Huang et al., 2010; Kennedy et al., 2010). For the purpose of change detection in the next step, image stacking was performed independently for each period to keep all the observations in the subsequent analysis. Then the pixels covered by cloud were removed from the MODIS and GIMMS NDVI time stacks according to the quality assurance flags of the two datasets and spline interpolation was adopted to create a per-pixel set of cloud-free image observations (a maximum time interval is set of 10). Finally, a complete 16-day NDVI profile for MODIS and half-month NDVI profile for GIMMS were generated for each period (e.g., the MODIS NDVI mosaics from 2000 to 2005 consist of 138 layers with

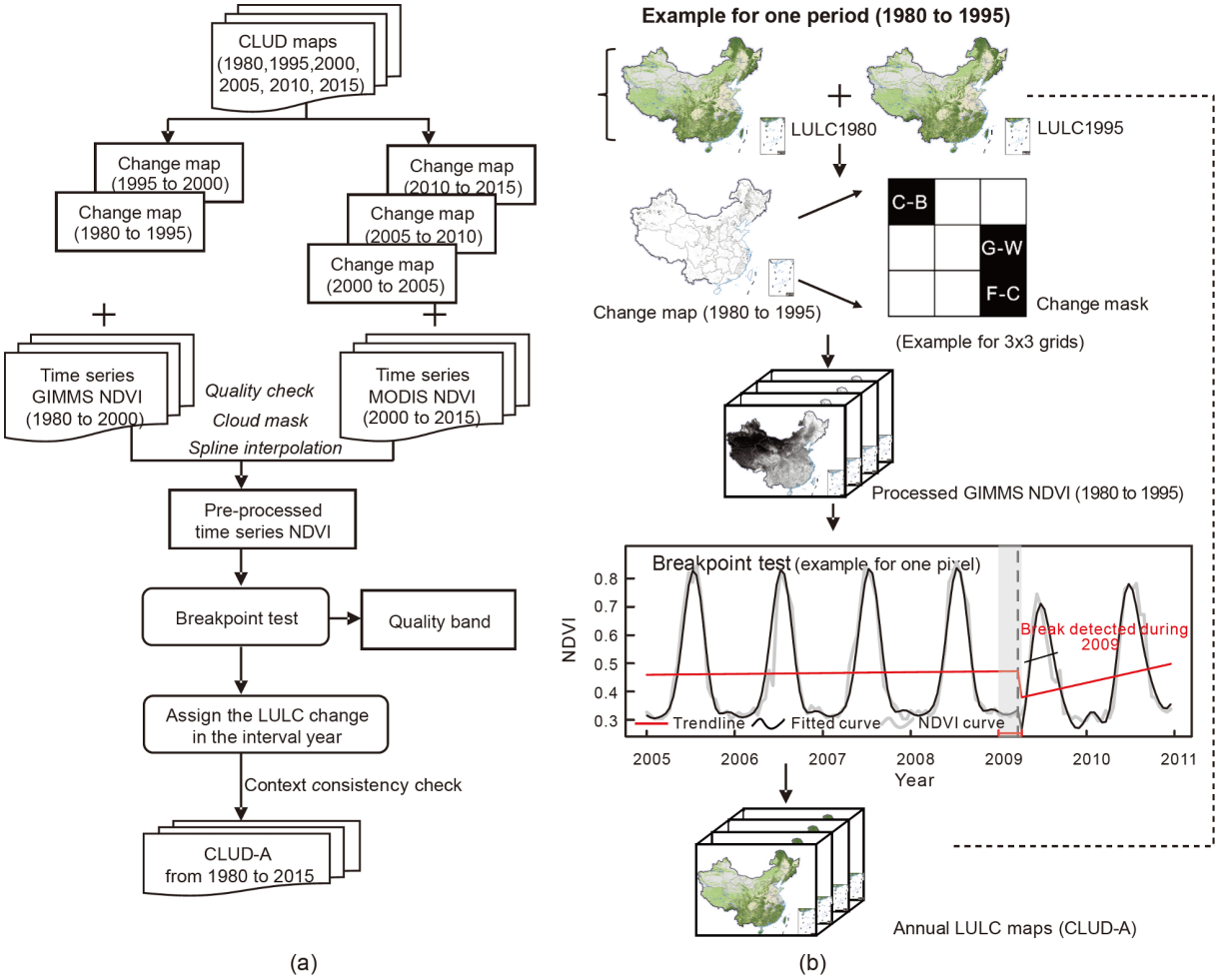

Figure 1 Workflow of annual land use/land cover (LULC) mapping process. (a) The flowchart, (b) an example for one period (1980–1995) including the change map extraction, NDVI dataset pre-processing, change time detection and annual map production. The 3×3 grid shows the enlarged example for 9 pixels while the line graph shows the example for one change pixel. The acronyms in the nine patches represents six primary land cover types (C: Cropland, F: Forest, G: Grassland, W: Water body, B: Built-up land, and U: Unused land).

23 observations per year for the 6-year intervals in each pixel).

2.2.2 *Change detection analysis*

To reduce the inter-annual inconsistency in annual classification and mitigate the huge workload in collecting training data, statistical based change-detection analysis was combined in the subsequent process with a new and simple methodology: given the change maps and "from-to" types for the five periods, the multi-time products can be expanded to annual LULC dataset by finding the exact change year among the intervals. Thereafter, change detection analyses were conducted in the pre-processed time-series (resized MODIS and GIMMS NDVI at 30 m resolution) profiles during different time periods for every change pixel (i.e., P1: 1980–1995, P2: 1995–2000, P3: 2000–2005, P4: 2005–2010 and P5: 2010–2015) to find the change year.

Change detection algorithms have been widely used to detect abrupt and subtle forest changes using different methodologies including differencing with thresholds (Huang et al., 2010; Jin et al., 2017), temporal segmentation (Kennedy et al., 2010) and statistical boundary analysis (Verbesselt et al., 2010b; Zhu and Woodcock, 2014). A comparison suggested that most of the algorithms reach high consistency in detecting significant variance (Cohen et al., 2017) and the season-trend model performed better than the seasonal-adjusted approaches in detecting the breakpoints (Forkel et al., 2013). Since the target land cover change occurs in six general LULC types with significant spectral variation, here we used BFAST, which considers the seasonality and noise of the NDVI time series, to identify the change time during each period.

The BFAST algorithm was originally proposed by Verbesselt et al. (2010a, 2010b) for monitoring forest disturbance using time-series MODIS NDVI data. It has since been modified and applied in all biomes at global and regional scale using different sensors including AVHRR, MODIS and Landsat (de Jong et al., 2012; DeVries et al., 2015; Verbesselt et al., 2010a), but has not yet been applied to all-type land cover types. Since a detailed description of the algorithms was given in (Verbesselt et al., 2010b, 2012), only a brief overview is presented here. The algorithm integrates a decomposition model which decomposes the time series into trend, seasonality and residuals components with an iterative algorithm to detect break points using structural change methods (Bai and Perron, 2003; Zeileis, 2005). The decomposition model can be expressed as

$$Y_t = T_t + S_t + \mathrm{e}_t,\ (t = 1, \ldots, n), \quad (1)$$

where Y_t is the observed value at date t. T_t is the trend component fitted by piecewise linear models, S_t is the seasonal component expressed by harmonic seasonal models, and e_t is the noise component which represents the remaining variation beyond seasonal and trend components. These trend and seasonal models were fitted to sections of time series according to the changes that had occurred and detected break points. In the iterative procedure, the ordinary least squares residuals-based moving sum test (Zeileis, 2005) was used to test whether there were one or more breakpoints. Then the trend and seasonal models were iteratively fitted to sections of the time series to find the position and number of the break points, which was determined by minimizing the residual sum of squares and information criterion during the iterative procedure following the multi-structural change detection (Bai and Perron, 2003). The BFAST algorithm is free of parameterization but requires a maximum number of breakpoints (also regarded as the minimum time between breakpoints according to the length of given time series).

Since there is a low probability of frequent changes such as two or three conversions during the 5-year interval (e.g., forest-cropland-water or grassland-cropland-grassland-unused land), only one single change during each period was explored in our study, in line with the prior changes given by the change maps from the CLUD. Therefore, the maximum breaks was set to 1 without considering the multi-time changes within each period in the algorithm. Although more changes may have occurred during the 15-year interval from 1980 to 1995, only one change was considered due to the lack of reliable dense land cover maps. Figure 2 demonstrates an example of detecting the breaks using the BFAST algorithm for the conversions among three typical vegetation types which are easily confused (forest to grassland, grassland to cropland and grassland to forest). The different trajectory of NDVI cycles illustrates different vegetation conditions (e.g., cropland with a single and double-cropping practice). In general, although the NDVI cycle variation before and after the change differs among land cover types, the turning point when abrupt land cover change occurs can be captured using the BFAST algorithm. It is worth to notice that the performance of the change detection algorithm is affected by the cloud conditions during time periods for every change pixel. During 2000–2005, 2005–2010 and 2010–2015, changes were detected in areas with at least 13.5 (59.93%), 12 (52.45%) and 13 (57.65%) cloud-free observations annually (Figure S2). And all the pre-defined change pixels (30 m) within a coarse resolution pixel (8 km AVHRR or 250 m MODIS) have the same detected change results because of the downscaling of the coarse dataset. The impact of downscaling is more significant in AVHRR data of ~50000 30 m pixels within one coarse pixel compared with 64 pixels of MODIS NDVI.

2.2.3 *LULC updates for the missing years*

The final step is the land cover updating for the missing years in each period. According to CLUD and the change maps for the five periods, there were two cases when LULC maps

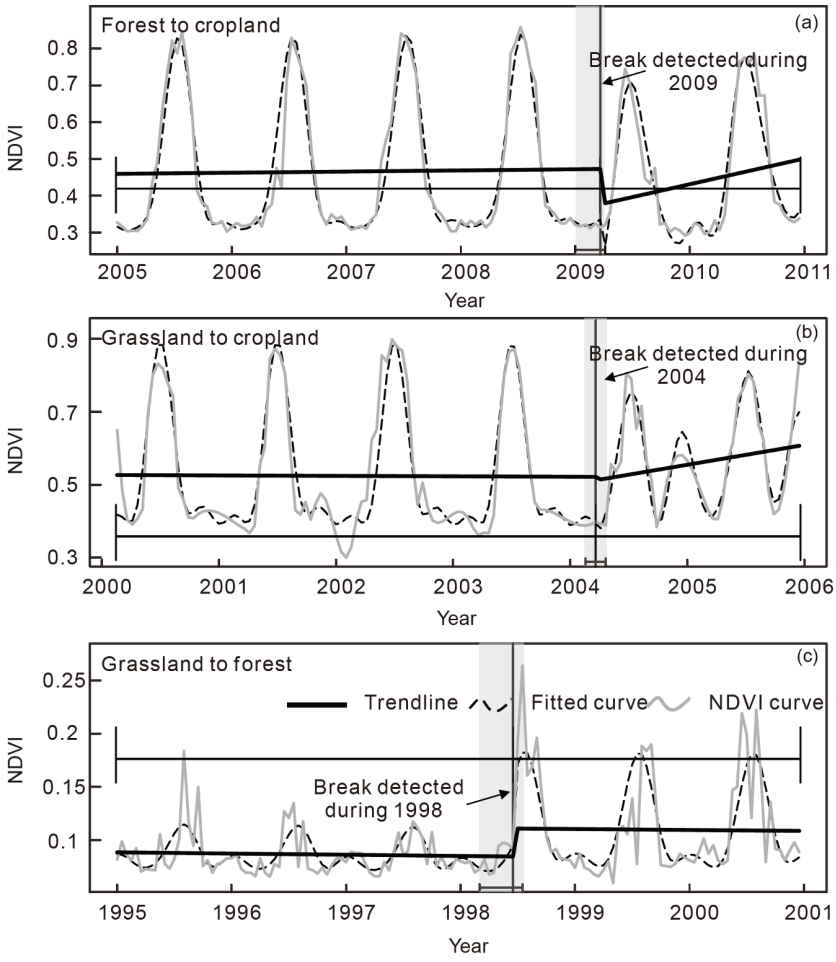

Figure 2 The sensitivity of MODIS ((a), (b)) and GIMMS NDVI (c) time series in identifying the change of vegetation types. (a) Location: 41.27°N, 120.62°E, the NDVI cycles differ after change occurred. The peak value of the MODIS NDVI curve for forest (before 2009) is higher than the subsequent curve, and the land cover type has changed to cropland. (b) Location: 50.21°N, 126.06°E, a double peak is presented in MODIS NDVI temporal files after 2004, which indicates the double cropping system after the conversion from grassland to cropland. (c) Location: 40.41°N, 79.65°E, the wave shape of grassland and forest type is distinguishable in the GIMMS NDVI profiles. The grey lines are pre-processed NDVI curve, the black dash lines are the fitted NDVI after iterative procedure and the black solid lines are the trend for the pre and prior segments before and after the change occurs. The break detected date is also given in the three examples with confidence interval of the date.

were updated in the intervening years as followings.

(1) For the unchanged area in the change maps, the land cover types L_1 and L_2 were consistent at the start (t_1) and the end (t_2) year of the 5-year period, therefore, the land cover types of the masked area in the missing period remained unchanged in the gap years (the same as L_1).

(2) For the change pixels with different L_1 and L_2, the exact change year (t_i) for each pixel in every period was derived from the change detection analysis in Section 2.2.2. Then L_2 was allocated from t_i to t_2 and L_1 was assigned before t_i (t_1 to t_i) according to the break date. For example, if a change pixel was grassland in the 2000 CLUD map and then turned to cropland in the 2005 CLUD map with a detected break year at 2004, then the land cover type from 2000 to 2003 would remain grassland whereas in the following two years would be updated to cropland. Thereafter, the LULC maps were updated for the intervening years in every period and original annual LULC datasets were generated.

Because the update of the LULC maps in the gap years was conducted separately for each period, there may be some false change detection among the different periods. For example, multiple changes in two successive years may occur if the changes were detected both in the end year of the previous period and the start year of the next period (i.e., cropland in 2004 is converted to forest in 2005 and then converted to cropland again in 2006). Here we adopted time-series filtering as recommended in annual land-cover maps produced by the European Space Agency Climate Change Initiative project at 300 m (ESA-CCI300). Each change had to be consistent for more than 2 years and was filtered if successive changes were detected (Defourny et al., 2017). Apart from annual LULC maps, quality maps were also produced based on the number of cloud-free NDVI values in each period, the spatial resolution of the dataset (250 m or

8 km), the length of each period (5-year or 15-year) and the same breaks detected by the different break test approaches included in BFAST (The ordinary least squares residuals-based MOving SUM test (OLS-MOSUM), the supremum of a set of Lagrange multiplier statistics (SupLM) and the Bayesian information criterion test (BIC) (Zeileis, 2005)).

2.2.4 Evaluation

Because of the huge workload and difficulty in collecting annual validation samples from 1980 to 2015 over the whole of China, the evaluation of CLUD-A was conducted by three independent validation sample datasets, which were aimed at assessing CLUD-A in temporal, spatial and change dimensions.

(1) The first was a fixed sample set which aimed to evaluate annual mapping accuracy of CLUD-A for the entire timespan. This independent validation sample set was from a published study for the rapid urbanization of Beijing (BJ-sample (Li et al., 2015)). This sample set contains 400 fixed test samples (including forest (25.85%), cropland (24.88%) and impervious (49.27%)) and a long time span from 1984 to 2013. In total, 12000 samples (400 samples×30 years) were used to validate CLUD-A in Beijing. This sample set was collected mainly based on high resolution images from Google Earth and NDVI time series.

(2) The second sample set was extracted from the first all-season training and validation sample sets for global land cover mapping (Li et al., 2017), which is used to evaluate the mapping accuracy in the spatial dimension for the whole of China (Here we named it the three-year China sample set). This sample dataset contains ~90000 training and ~35000 validation samples interpreted on Landsat 8 with records of the date of image acquisition (interpreted from 2013 to 2015), spectral reflectance for each season, and level of interpretation uncertainty and sample sizes (3×3, 9×9, 17×17, 33×33, 1 unit =30 m). All the samples were interpreted by 13 image interpreters using seasonal Landsat images, MODIS EVI time series, monthly temperature and precipitation as well as the Google Earth images. In addition, the hexagon-based equal-area stratified random sampling scheme guaranteed the random and even distribution of samples.

We selected all the samples located in China with high confidence according to the confidence level of the validation sample set and a sample size of 30 m×30 m and then converted them to the CLUD classification system. In total, 532 and 6760 samples for 2013 and 2014 were used to validate the updated 2013 and 2014 maps in CLUD-A. The 5376 samples for 2015 were also used to assess the original CLUD for 2015 as a comparison to see whether there had been a decline of mapping accuracy in the updated years. Meanwhile, we also compared the mapping performance of CLUD-A with the other available continuous annual datasets, MODIS land cover product (MCD12Q1) and ESA-CCI300 (Defourny et al., 2017).

(3) The third sample set focused on evaluating the change year identified by the change detection analysis. We used the 41 samples which were located in the change regions in our change maps from the 2010 global validation samples set (Zhao et al., 2014) and then visually interpreted the exact change years using very high-resolution (VHR) imagery from Google Earth and Landsat time series (in the early stage without VHR images). The detected change years using the change detection algorithms were later compared with the actual change year for these test samples to assess the accuracy of CLUD-A within each period. Here, we adopted a confidence interval of ±1 years in the comparison in view of the uncertainty in visual interpretation of the change year (Dara et al., 2018).

Apart from the quantitative comparison using the validation sample sets, visual comparison in areas with rapid changes (e.g., urbanization, cropland changes and deforestation) was conducted to show the change performance using several annual land cover datasets including Beijing urbanization datasets (Li et al., 2015), ESA-CCI300 (http://maps.elie.ucl.ac.be/CCI/viewer/) (Defourny et al., 2017), MODIS land cover products at 500 m (MCD12Q1, https://lpdaac.usgs.gov/products/mcd12q1v006/) (Friedl et al., 2002) and 30 m forest loss map from Hansen et al. (2013). The classification systems of ESACCI-300 and MCD12Q1 were converted to the CLUD-A classification system based on the cross walking table in supplementary (Table S1).

3. Results

3.1 Annual LULC change in China from 1980 to 2015

Using the CLUD, and combining the coarse satellite datasets with the change detection method, we developed annual land use/land cover datasets (CLUD-A) from 1980 to 2015 (Figure 3). The four enlarged maps illustrate the LULC dynamics over the past three decades with examples from the complete years. For instance, an expansion of built-up land occurred in the Northern China Plain, Yangtze River Delta, Pearl River Delta and the Sichuan Basin.

Details of the spatial-temporal dynamics of some typical land cover conversions, both continuous or abrupt, are enlarged and given in Figure 4 (i.e., cropland expansion, afforestation, reclamation, deforestation, rapid urbanization and reservoir construction). The graded colour changes refer to different change years over the study period and the Google Earth images show the land change dynamics. In Figure 4, each sub-figure represents a continuous or abrupt change for one land cover class, including (1) cropland expansion in Qiqihaer on the SanJiang Plain, north-east China (Figure 4a); (2) afforestation in Yan'an, Shanxi Province following the re-vegetation project in China (as suggested by

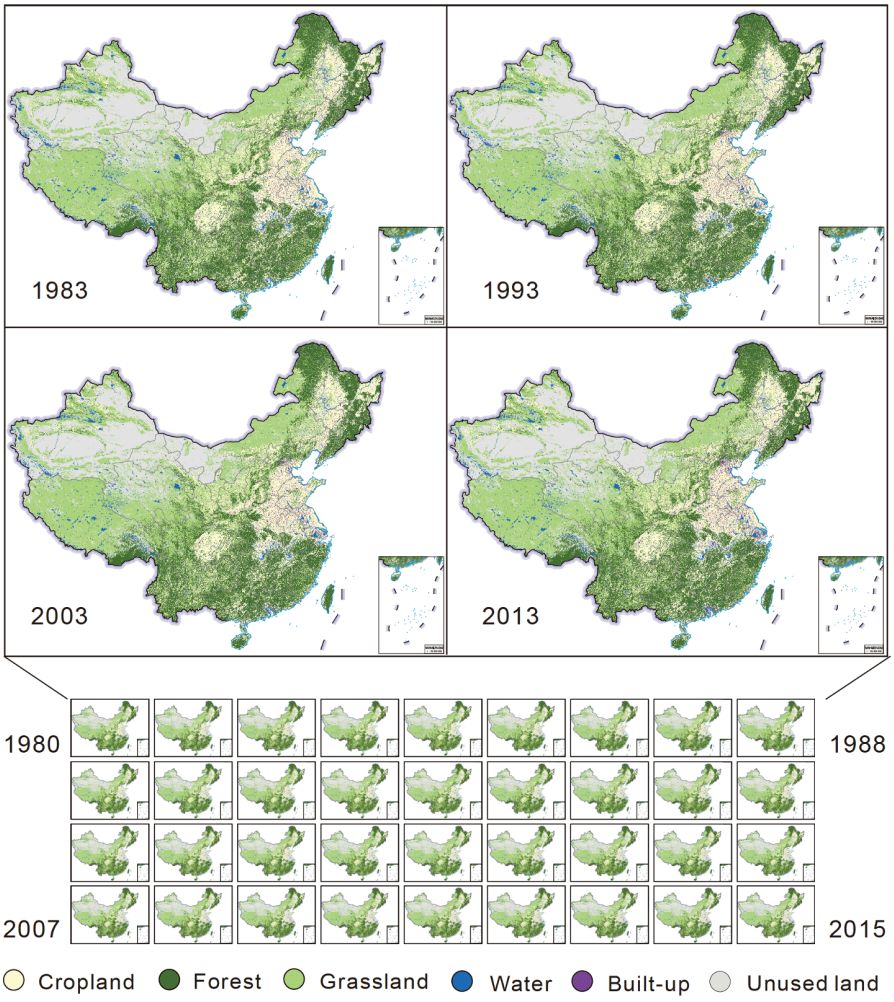

Figure 3 Annual land use/land cover dataset for China (CLUD-A) from 1980 to 2015. The four selected years (1983, 1993, 2003, 2013) are enlarged.

Google Earth images in Figure 4b, the artificial forests were planted in arcs); (3) the transformation of unused land, also known as desert reclamation in Peitun in the Altay region (Figure 4c). This area is an arid and semi-arid region in north-west China, and the major land use pattern is the development of oasis agricultural areas based on water from the Ulungur Lake in the north-west; (4) forest logging activities in Heihe city in north-east China during the early stages after reform and opening-up (Figure 4d) when expanses of forest were cut down for agricultural areas; (5) significant built-up land expansion and rapid urbanization process in the Yangtze River Delta (Figure 4e); and (6) abrupt water expansion in 2004 in Yichang City, Hubei Province (Figure 4f) following the establishment of the Three Gorges Project and water filling since 2003.

Figure 5 demonstrates the area change for each land cover type in China by year from 1980 to 2015. The dashed vertical lines refer to the year with CLUD while the rest are the interpreted CLUD-A. The yearly area changes and trend for each land cover type in China from 1980 to 2015 were also successive and similar to the original CLUD. These changes prove the value of using existing CLUD and time-series coarse datasets in deriving long-term LULC maps at yearly scale in regions without frequent Landsat observations.

Overall, the land cover change between 1980 and 2015 can be summarized as: (1) A rapid increase of built-up land (45.73%) compared with the 1980s; (2) a slight but continuous increase of water by 0.91 million ha (3.34%); (3) a successive decrease of grassland and unused land (−1.86% and −0.86%, respectively); (4) a 2.68 million ha (1.51%) cropland increase from 1980 to 2000, then a decrease after 2000 (−2.14 million ha); (5) a significant decreasing trend after 1995 in forest type but recovered since 2000. The total area of forest was relatively stable from 1980 to 1995, with a 0.18% increase in the first 5 years and a 0.08% decrease in the following 10 years. Then, forest experienced a dramatic decline from 1995 to 2000 (−0.46%). An increase of forest area was found after 2000 because of the implementation of six key forestry projects (Liu et al., 2014). However, the forest resources have shown a declining trend over the last

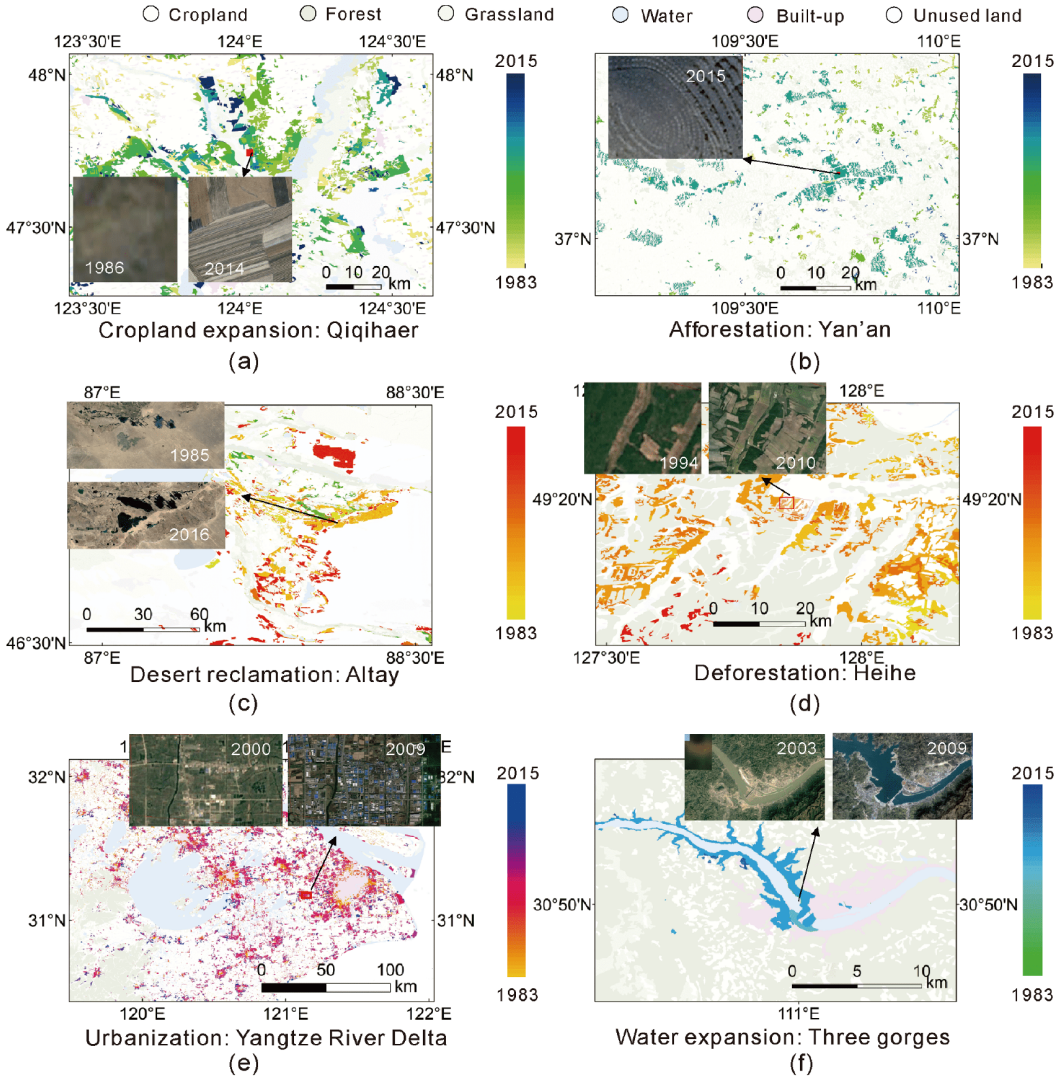

Figure 4 Typical annual land use/land cover (LULC) changes over past decades. (a) Cropland expansion in SanJiang Plain, north-east China, (b) tree planting detected under the Three North Project, (c) desert reclamation in the south-east of Ulungur Lake, Altay Prefecture, Xinjiang, (d) forest logging activities in Heilongjiang Province, (e) urbanization captured by annual results in the Yangtze River Delta region, (f) water expansion caused by the construction of the Three Gorges Project.

5 years (2010–2015).

Annual change rates also showed a similar trend to the net land cover change amount in quantity. Built-up land shows the highest rate of increase among all the land cover types at (0.21 million ha yr^{-1}) over the past 35 years, with a greater acceleration in the last 15 years (0.37 million ha yr^{-1}) than in the previous 20 years (0.08 million ha yr^{-1}). A significant and continuous decline trend was found in grassland (−0.16 million ha yr^{-1}), followed by unused land (−0.05 million ha yr^{-1}).

3.2 Mapping performance of CLUD-A

3.2.1 Mapping accuracy from temporal, spatial and change perspectives

The mapping performance of CLUD-A was evaluated from three temporal, spatial and change perspectives. First, annual BJ-sample set from 1984 to 2013 which almost covers the entire time span gives a clue to the mapping performance in the updated years. Annual average accuracy (average of user's accuracy (UA) and producer's accuracy (PA)) for cropland, forest and built-up land was 72.10%, 78.93% and 91.89%, respectively. Figure 6 illustrates annual change of the user's and producer's accuracy for these three land cover types. The dots mark the accuracy derived from CLUD from 1995, 2000, 2005 and 2010 while the lines show the accuracy of the updated years. Built-up land showed the highest accuracy with limited fluctuations while cropland showed the opposite pattern. The accuracy (average of UA and PA) of the built-up land (91.89%) in our studies is also comparable to the annual mapping results based on Landsat observations (94%) (Li et al., 2015). Forest reached a higher average ac-

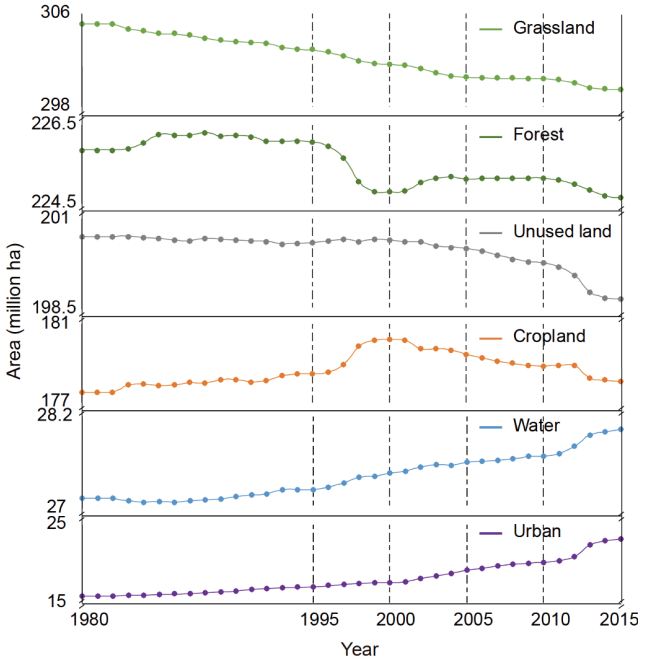

Figure 5 Area change in different land cover classes in China from 1980 to 2015. The fluctuations for each land cover type are enlarged using the different range of *y*-axis.

curacy (80.49%) before 2000 and had a lower accuracy after 2000 (76.42%). Cropland and built-up land show the higher PA than UA, which indicated the underestimation of the two land cover types (particularly cropland) in the mapping results. According to Figure 6, there is no significant difference in the mapping accuracy among the four CLUD maps and the updated intermediate years in CLUD-A (a differences of 0.95%, 1.19% and −0.80% for cropland, forest and built-up area, respectively).

Second, the three-year China sample set with 532, 6760 and 5376 samples for 2013, 2014 and 2015 located in China, were used to validate the 2013, 2014 and 2015 maps in CLUD-A. UA and PA for each land cover type are shown in Table 1. The overall accuracies were relatively stable over the three years with a 0.5% fluctuation. The classification crosswalk to map one classification to another may have caused the lower mapping accuracy (~70–78%) compared to the reported mapping accuracy (90%). For example, marsh covered by vegetation was change to unused land according to the cross walking table (Table S1) in CLUD-A, which is classified as vegetation in the original classification systems. There is no shrub land or wetland category in CLUD-A, which may have caused some confusion in grassland and unused land (Table 1). However, the stability of inter-annual accuracy over the whole of China gives a clue to the mapping quality for the updated missing years.

The change time accuracy, validated by the third change dataset, showed 75.61% agreement with the actual year from high and medium resolution images (2/3 of the detected change year matched the interpreted change time while 1/3 was within a 1-year interval). The deviation of the years is shown in Figure 7. The validation samples from different periods are shown in different colours. Further, the change year is more accurate after 2000 when MODIS data of a higher resolution was used and larger deviations (>2 years) were mainly found in the early stages of the study period with the longest, 15-year interval between the two CLUD maps (i.e., the sample with the largest deviation was 7 years from the 1980s to 1995) (for the temporal and number distribution of the deviations, please refer to Figure 7). This is also included in the quality bands where the pre-2000 data updated using coarse GIMMS data were of lower quality.

Figure 8 shows the direct comparison of the change maps with the high-resolution images available from Google

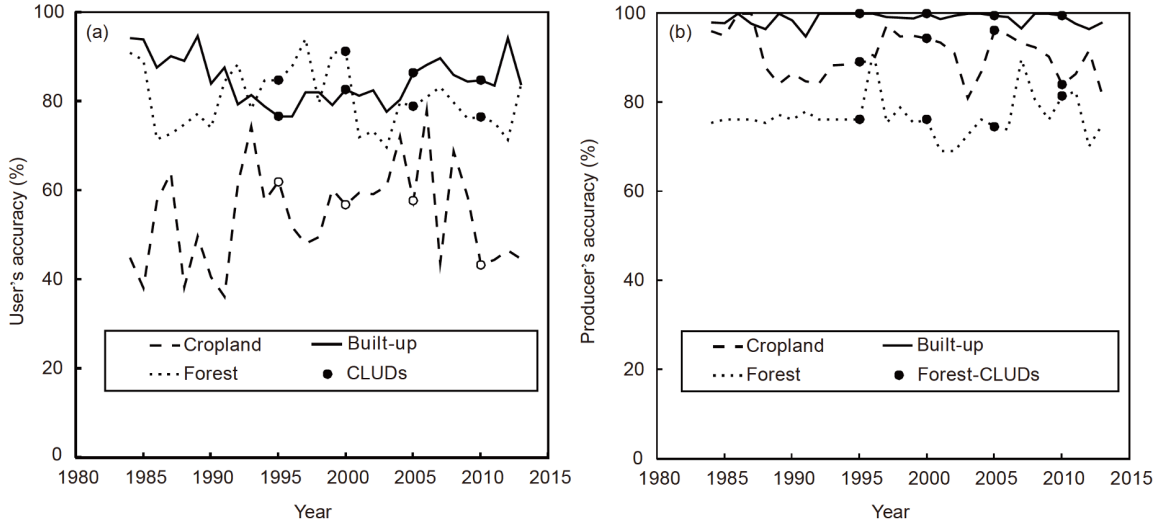

Figure 6 Annual mapping accuracy (user's accuracy and producer's accuracy) of cropland, forest and built-up land types in Beijing using validation samples from 1984 to 2013 (Li et al., 2015). The lines show the accuracy of CLUD-A from 1984 to 2013, while the dots mark the accuracy derived from CLUD in 1995, 2000, 2005 and 2010.

Table 1 Accuracy assessment using three-year China sample set for all the land cover types in CLUD-A for 2013, 2014 and 2015[a)]

Year	2013		2014		2015	
	UA (%)	PA (%)	UA (%)	PA (%)	UA (%)	PA (%)
Cropland	66.23	75.19	76.26	77.78	78.26	78.55
Forest	79.41	78.03	75.89	79.54	76.31	79.55
Grassland	50.00	53.42	45.00	64.12	43.40	63.10
Water	88.24	76.92	83.29	78.67	81.37	80.98
Built-up area	81.82	72.58	80.72	77.37	80.69	78.65
Unused land	50.00	38.46	83.75	60.68	85.71	61.65
OA (%)	72.18		71.60		72.21	

a) UA, user's accuracy; PA, producer's accuracy; OA, overall accuracy.

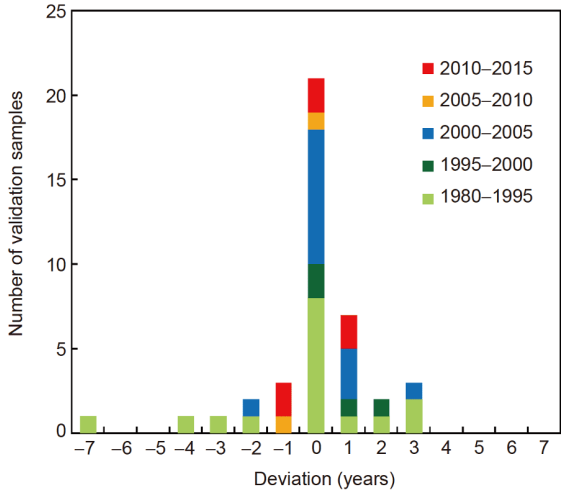

Figure 7 Deviation of detected change years from the reference change point dataset (interpreted from Google Earth and Landsat images). Negative values in the *x*-axis mean that the detected change years were earlier than the actual change years and positive values show the opposite.

Earth, which document the change process. The four selected regions represent four different land use changes. Overall, most of the changes were captured within the range defined by the Google Earth time lapse images, as can be seen from the detected change years in the highlighted regions (light blue shapes).

3.2.2 *Comparison with other LULC products*

We first compared the change of built-up land from our CLUD-A with the impervious area from a published paper (Li et al., 2015), which studied annual urbanization process in Beijing from 1984 to 2013. Annual datasets for Beijing in Li's study were classified using Landsat datasets at 30 m resolution. The overall urban expansion pattern in Beijing is similar between the two datasets (Figure 9), with more built-up areas concentrated in the plains in the southwest of Beijing and urban expansion from the centre to the outskirts. We further overlaid the detected change years in the 5 periods of CLUD-A (P1: 1980–1995, P2: 1995–2000, P3: 2000–2005, P4: 2005–2010 and P5: 2010–2015) and urbanization year from Li's datasets (1984 to 2013). Among the overlapped change area, 22.97%, 34.69%, 27.04% and 29.68% of the area has the same change time, while 75.34%, 75.19%, 70.88% and 76.62% of the area was in 1-year intervals during 1995–2000, 2000–2005, 2005–2010 and 2010–2013. The largest differences were found in years between 1983 to 1995, where only 26.77% of the change year detected in CLUD-A coincided with Li's datasets within 1-year intervals.

The large discrepancy is probably contributed by the application of the coarse GIMMS NDVI data and the change detection algorithm over the longest studied temporal period (1980–1995). The visual comparison in Figure 9b shows the similar results, the built-up areas vary in the earlier periods (dark blue and green area) and the expansion year was largely influenced by the use of the coarse dataset (the uniform color in Figure 9b(ii) compared to Figure 9b(i)). The land parcels, however, showed consistent change year in recent periods in the two datasets. Generally, CLUD-A shows homogeneous parcels with less "salt and pepper" because of the manual interpretation of the CLUD.

We also compared our mapping accuracy with the other two time-series land cover datasets, ESA-CCI300 and MCD12Q1 using the three-year China sample set. Table 2 lists the results, including the overall accuracy, UA and PA of the eight land cover types of the three datasets. Overall, the CLUD-A (72.00%) and ESA-CCI300 (72.86%) had a similar accuracy, which is ~7% higher than MCD12Q1 for the three years. It is worth noting that the validation dataset was different for each of the three products and the translation/fusion of different classifications may have caused the biases. The accuracy of the three datasets also showed a similar pattern: built-up land and forest had the highest accuracies among all three datasets (>75%), followed by cropland, water and unused land, and the lowest accuracy was found in grassland (around 55%). The mapping accuracy of water and cropland in CLUD-A and ESA-CCI300 was higher than that of MCD12Q1, which is probably because of the higher spatial resolution.

The two selected areas in Figures 10 and 11 depict the

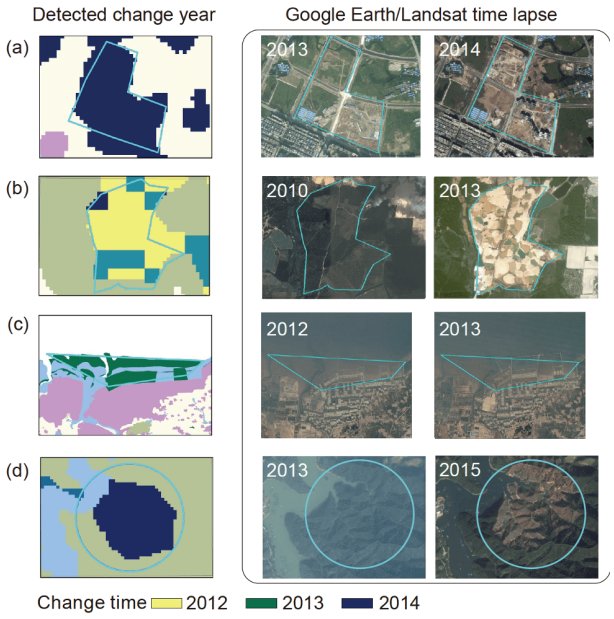

Figure 8 Visual comparison of the detected change years (the first column) with the images from Google Earth and Landsat (the second and third column). The highlighted areas with blue shapes were the change regions. The four examples demonstrate different land cover changes including (a) the conversion from cropland to urban area, (b) change from forest to cropland, (c) sea reclamation with construction over the sea and (d) change from forest to grassland after logging activity.

disagreement of forest and cropland (both by extent and change years) among the several existing continuous LULC datasets. Figure 10 shows the forest extent and loss year in a region of north-east China among five annual datasets, the 500 m MCD12Q1 product, the 300 m ESA-CCI product, the 30 m forest loss map from Hansen et al. (2013), the 30 m Landsat-based annual North-East China maps from Zhao et al. (2019) (Figure 10) and our CLUD-A. The base maps were the original 2001 LULC results for the five datasets. The loss of forest was extracted and shown from the original all-type LULC datasets as a comparison. All the different land cover systems were unified and converted to CLUD-A. The forest cover extent (the light green) is similar in the three 30 m (or nominal 30 m) datasets, with more forests found in CLUD-A and the least in Hansen's data, while there is less detail at the edge of forests in the coarse datasets (MCD12Q1 and ESA-CCI300). However, the forest loss map differs in all five products in terms of change range and year, with most forest loss found in Zhao's maps and the least in Hansen's data.

In addition, the cropland extent and change years in central China were also compared with the 500 m MCD12Q1 product and the 300 m ESA-CCI300 product (Figure 11). Figure 11 shows examples of two agricultural regions, one with cropland change (the first row) and the other without significant changes. In the first example, the marked area used to be cropland before 2007 and then turned to water in 2008 because of a change in the river courses. However, the change process was not captured in the ESA-CCI300 product and the river was wrongly classified as grassland in the two coarse datasets. The regular cropland area in the second example is wrongly classified as forest in the MCD12Q1 product, causing incorrect recording of cropland expansion in this area between 2002 and 2015.

4. Discussion

It is a great challenge to obtain annual LULC for the whole country at 30-m resolution and subsequent change information. At national and continental scale, land use areas

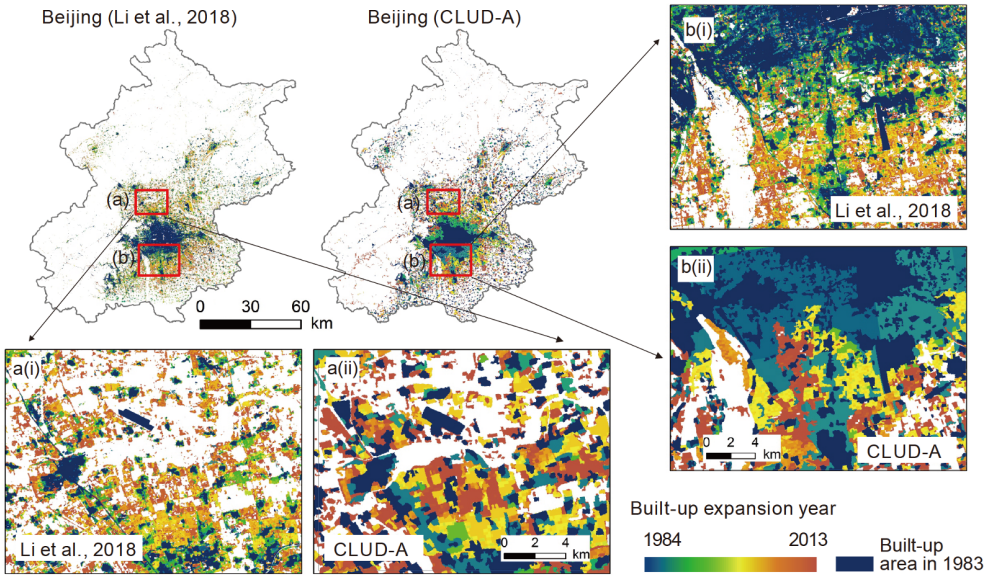

Figure 9 Comparison with the 30-m urbanization datasets from Li et al. (2015) in Beijing from 1984 to 2013.

Table 2 Comparison of mapping accuracy in the three land cover datasets, ESA-CCI300, MCD12Q1 and CLUD-A (our results)[a)]

Types	PA (%)								
	Our results			ESA-CCI300			MCD12Q1		
	2013	2014	2015	2013	2014	2015	2013	2014	2015
Cropland	75.19	77.78	78.55	87.97	83.82	83.41	34.59	57.06	59.85
Forest	78.03	79.54	79.55	82.56	76.61	76.76	98.27	84.43	83.08
Grassland	53.42	64.12	63.10	57.53	63.18	62.94	56.16	75.48	76.32
Water	76.92	78.67	80.98	71.79	73.20	73.62	30.77	40.36	41.00
Built-up area	72.58	77.37	78.65	72.58	75.44	75.64	72.13	64.76	65.47
Unused land	38.46	60.68	61.65	7.69	58.66	61.78	38.46	72.46	72.07
Types	UA (%)								
	Our results			ESA-CCI300			MCD12Q1		
	2013	2014	2015	2013	2014	2015	2013	2014	2015
Cropland	66.23	76.26	78.26	59.69	59.49	61.18	76.67	73.08	73.78
Forest	79.41	75.89	76.31	85.54	83.70	84.34	54.84	61.41	63.34
Grassland	50.00	45.00	43.40	70.00	43.76	43.06	56.94	44.31	42.72
Water	88.24	83.29	81.37	98.25	95.75	93.97	88.89	95.20	95.83
Built-up area	81.82	80.72	80.69	88.24	87.65	88.72	83.02	80.39	80.47
Unused land	50.00	83.75	85.71	100.00	92.91	93.22	55.56	90.76	91.48
OA (%)	72.18	71.60	72.21	75.89	70.91	71.77	62.15	67.52	68.07

a) The accuracies for the specific land cover types are the mean of the producer's and user's accuracy. OA refers to overall accuracy.

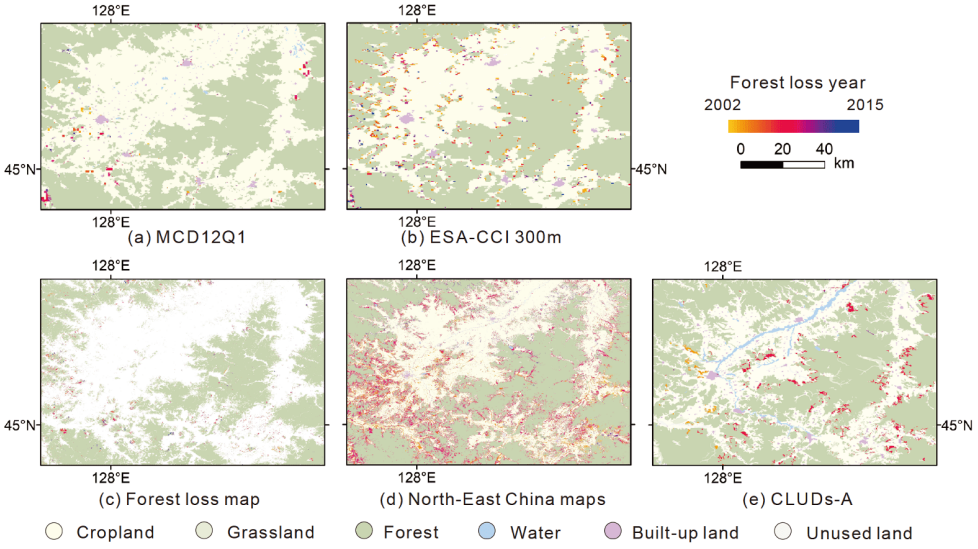

Figure 10 Example of disagreement in the extent and year of forest loss in the five datasets from 2002 to 2015 in North-East China. (a) MCD12Q1, 500 m; (b) ESA-CCI 300, 300 m; (c) forest loss map from Hansen et al. (2013), 30 m. A 50% threshold was used to derive the forest extent in 2001 using the tree cover proportion map; (d) annual North-East China maps from Zhao et al. (2019), 30 m; (e) CLUD-A, nominal 30 m.

are commonly given in multi-decadal or yearly statistical books, which lack spatial information and sometimes is contradictory with land surveys (Smil, 1999). Satellite-based studies provide a cost-saving and labour-efficient way to continuously monitor LULC changes. But the long-term annual information extraction at tens-of-meter resolution (e.g., 30 m) is limited by the insufficient Landsat images (particularly in historical change analysis, (Yu et al., 2015)) and mostly focuses on single-type conversions like forest and impervious categories (Hansen and Loveland, 2012). In this study, we provide a new prototype for obtaining nominal 30 m dataset by updating the discrete LULC maps (CLUD) to annual land use/land cover datasets (CLUD-A) using a generic change detection approach (BFAST) and time-series NDVI data with dense temporal but coarse spatial resolution. This method integrates the strengths of multiple satellite

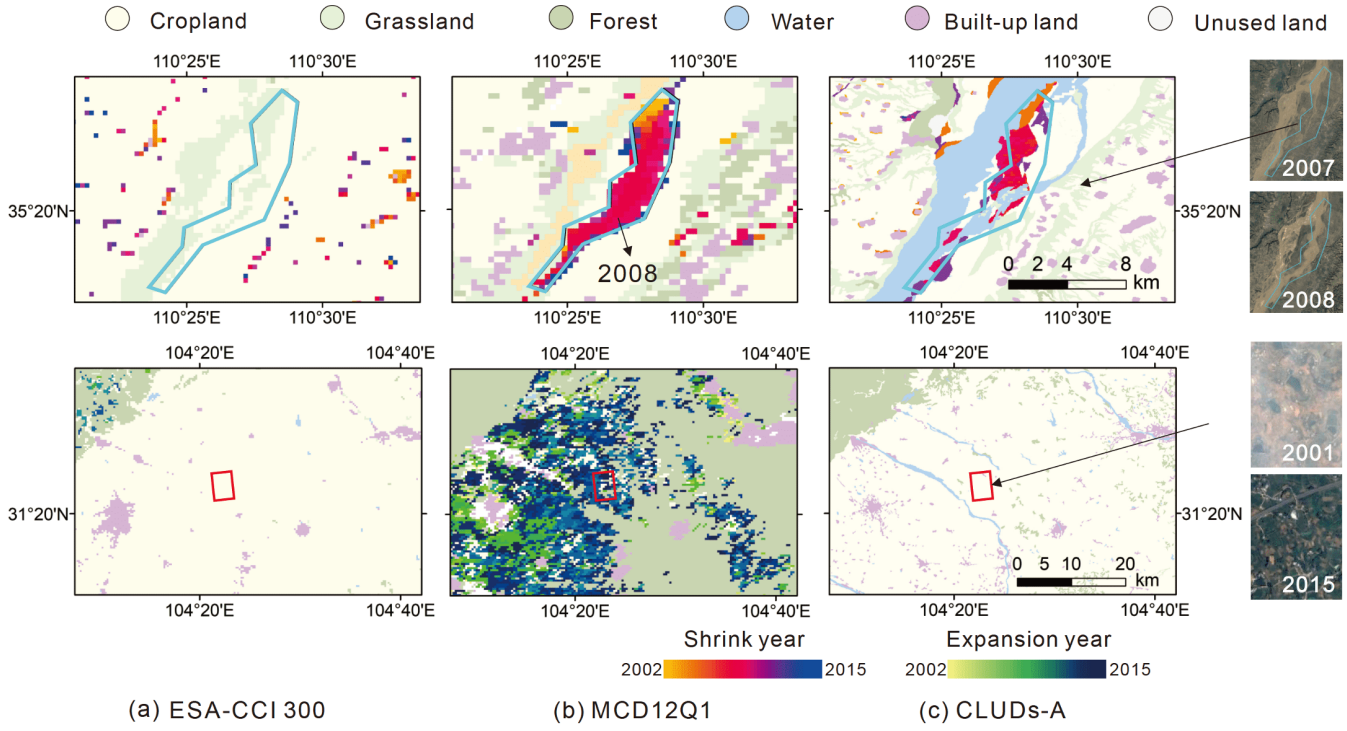

Figure 11 Examples of disagreement for cropland change from 2002 to 2015 in the three datasets. (a) ESA-CCI 300, 300 m; (b) MCD12Q1, 500 m; (c) CLUD-A, nominal 30 m. The first row shows cropland reduction by a riverside because of the changes in the river. The second row is a cropland area without significant changes.

data, a change detection algorithm and existing LULC datasets at fine resolution.

In many regions around the world, apart from the United States, the coverage of cloud-free Landsat images is limited, particularly in earlier years such as the 1990s. An alternative way to trace historical LULC changes is required. One potential way is to integrate coarse MODIS and GIMMS data. Here we fully utilised the change information and prior knowledge from the 30 m mapping results (CLUD) to reduce the errors which may have been introduced by different sensors, coarse resolution, false changes and misclassification. For example, using coarse datasets (500 m and 300 m) alone causes a loss of spatial detail while combining the fine, reliable CLUD maps with high accuracy and coarse MODIS/GIMMS data reduces the biases (Figure 10a, 10b, Figure 11a, 11b compared to Figure 10e and Figure11c). Also, the stable mapping accuracy for the whole of China, annual maps in Beijing and the change detection performance all suggest the potential for using this approach to monitor long-term LULC changes. More importantly, this prototype can be transferred and applied in other regions with multiple discrete LULC datasets such as the West Africa Atlas for West African countries from 1975 to 2013 by the U.S. Geological Survey (Cotillon, 2017), the CORINE land cover datasets for European Countries at 6-year intervals from 1985 to 2018 (Feranec et al., 2016), National Land Cover Database Land Cover Collection for the U.S. at 5-year interval from 2001 to 2016 (Jin et al., 2017) and other regional datasets. It is important to notice that the approach is dependent on the reliable CLUD datasets (with >90% accuracy) and annual mapping accuracy will be decreased with less reliable base maps.

Another major concern in long-term annual LULC mapping is discontinuity and false changes detected in annual classification results. As is shown in Figure 10d, the overestimation of forest loss largely contributed to the false changes detected. A common practice is temporal filtering in post-processing to ensure context consistency (Cheng et al., 2019; Xu et al., 2017). However, these filtering rules, based on assumptions such as one-way expansion, are only suitable for some land cover types (i.e., built-up and cropland) over several regions and the rules may vary in different regions. This method, combining change detection algorithm and discrete LULC datasets with given "from-to" types can be used to extract multi-directional land cover changes (e.g., cropland expansion and shrink) and in the meantime, guarantee context consistency.

Further, the potential of the change detection algorithm, BFAST in all-types of land cover change, has yet to be fully explored. Although the algorithm has been used in break detection in cropland and fire dynamics (Dutrieux et al., 2016; Permatasari et al., 2016; Quarfeld et al., 2016), the wider usage was in forest disturbance and recovery (de Jong et al., 2013; Watts and Laffan, 2014). However, since it can be applied to detect changes in trends and seasonal components for both abrupt and subtle changes, it can be applied in

monitoring the conversion from different land cover types with significant signal differences. And the prototype of combining the statistical-based change detection algorithm and LULC mapping is not limited in BFAST but other temporal analysis algorithms (e.g., trajectory based approaches like Landtrendr (Kennedy et al., 2010)) regarding characteristics and specific applications. With the increase of data volume, this approach can be applied to other satellite data sources such as dense Sentinel and Landsat data.

As a result, CLUD-A captured the total changes within each 5-year period and reduced the time lags between the actual change year and the mapping time since the changes may occur at any point during the 5-year period. For example, if a change in land cover type occurred in CLUD between 2000 and 2005, and the change detection analysis showed the change had occurred in 2004, then the time lag of the change would be defined as 1. The number of changes for each period and the distribution of time lags are shown in Figures 12a and 13b. For Period 2 (P2, 1995–2000) to Period 5 (P5, 2010–2015), the range of time lags were from 0 to 4. Period 1 (P1, 1980–1995) had the maximum time lag of 12 for the longest interval. It is not surprising that most of the changes (42.13%) occurred in P1 which covered the longest time span. However, only 4.3% changes occurred exactly in the mapping years of CLUD (as shown in Figure 12b), and the rest had time lags from 1 to 12 years.

While some challenges in annual LULC mapping were overcome, there were some uncertainties in this study. Since the original CLUD were at 30-m resolution, the use of coarse data (MODIS and GIMMS) at 250 m and 8 km resolution caused the loss of spatial information (all changed pixels within one coarse resolution pixel has the change in the same year) in identifying the sub-grid change years (as can be seen in Figure 9b(ii)) because there could be multiple change times in the sub-grids. This problem was partially solved by controlling the total changes using two CLUD maps at the start and the end of each period. However, the Further effort includes fusing multi-resolution satellite data which also requires a dense frequency of fine resolution datasets (Zhang et al., 2017). Although the fusing approach can improve the data volume to some extent, the fused time-series is not a good substitute for the real dense fine resolution satellite dataset. When conducting annual LULC mapping, attention should be paid to choose suitable satellite data for a specific purpose.

Another uncertainty originated from the change detection algorithm, BFAST. It is easy to capture significant changes (e.g., water to cropland) but it may take a long time to capture gradual change (e.g., land degradation such as forest to grassland and grassland to unused land) and thus difficult to identify the exact change year. The accuracy of a detected change year within a time series is also influenced by the signal-to-noise ratio (Verbesselt et al., 2010b). Cloud contamination and fluctuating poor data quality in some regions of the MODIS and GIMMS products reduces the amount of valid information and the detected change accuracy (particularly in cloudy region such as Yunnan Province (Figure S3c)). Thus, we provide a data quality layer based on the original satellite data quality. Also, the accuracy of this method was highly dependent on the original LULC datasets which provided change and "from-to" information.

CLUD has a high reported accuracy at 94.3%, but demonstrated a lower accuracy using the China validation sample set. The misclassified pixels could trigger cumulative errors in the next change detection process. We used CLUD as the base LULC maps for updating because, to the best of our knowledge, they are the most reliable LULC datasets in China with multi-time phases and the highest resolution. In this study, we assumed that bi-directional and multi-directional land use conversion would not happen in a 5-year period. In most circumstances, change of the land surface is a slow process which requires time but this assumption does not apply in all situations. Some rapid changes would not be picked up, such as the land cover dynamics before and after

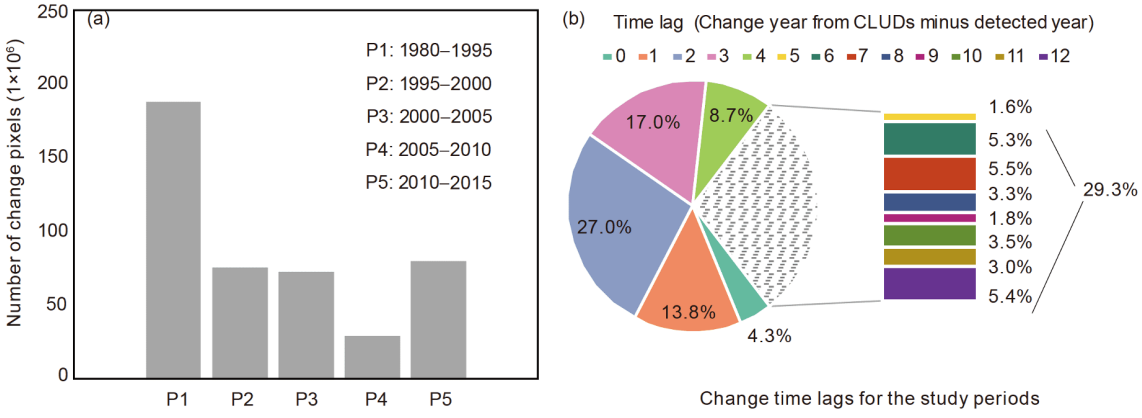

Figure 12 Number and distribution of detected change delays between continuous CLUD-A and discrete CLUD dataset with 5- and 15-year intervals. P1: 1980 to 1995, P2: 1995 to 2000, P3: 2000 to 2005, P4: 2005 to 2010, P5: 2010 to 2015. The time lags describe changes that occurred within the 5-/15-year intervals but were not captured by the discrete CLUD dataset because of the temporal resolution.

hurricane Katrina (Li et al., 2016). Further improvements could be made to capturing multiple changes in a given period and identifying the multiple "from-to" types using temporal segmentation and spectral fitting methods (Yin et al., 2018).

Overall, the proposed method can be used in several applications where there is a need to identify uncertainty and a potential deviation of 1 to 2 years for change dates. First, this dataset applied a basic method and suggested inputs which will be useful for further research. For example, this method can be either used in regions that require annual LULC maps where reliable discrete LULC datasets are available but without frequent Landsat observations (i.e., West Africa). Second, annual data can be used to evaluate the effect of government policies such as re-vegetation and serves to supplement statistical data which is labour-intensive to collect. When quantifying land-use change impacts on ecosystems, LULC datasets at fine spatial-temporal resolution can be used as better inputs in carbon cycle models. Generally, CLUD-A has the potential to describe the process of urbanization, deforestation, reclamation and water changes and could be further used in related specific disciplines.

5. Conclusions

In summary, this study developed a new approach for updating existing discrete CLUD products to a yearly CLUD-A product by integrating multiple satellite data and using a change detection algorithm. This prototype makes full use of the higher spatial resolution and longer time span of different satellite data sources and therefore, provides a potential for developing annual LULC datasets, particularly in areas with reliable discrete LULC datasets (e.g. CORINE programme for European countries) but insufficient Landsat observations (e.g., West Africa). By controlling the total changes using CLUD, the dataset showed a good performance in annual classification and change-detection accuracy (75.61%), which also suggest the use of generic BFAST algorithm in all-type LULC change detection. The developed CLUD-A provides insights and details on dynamic LULC changes for China from the perspective of remote sensing, reducing the time lags of detected changes compared to the discrete CLUD and can serve as a supplement for national statistics. Further application of the datasets includes, but is not limited to, regional carbon studies, urban planning, water and agricultural management, and policy evaluation.

Acknowledgements *This work was supported by the National Key R&D Program of China (Grant Nos. 2017YFA0604401 and 2019YFA0606601), the Tsinghua University Initiative Scientific Research Program (Grant No. 2019Z02CAU) and the Youth Innovation Promotion Association, Chinese Academy of Sciences (Grant No. Y4YR1300QM).*

References

Akiyama T, Kawamura K. 2007. Grassland degradation in China: Methods of monitoring, management and restoration. Grassland Sci, 53: 1–17
Bai J, Perron P. 2003. Computation and analysis of multiple structural change models. J Appl Econ, 18: 1–22
Bai Y, Feng M, Jiang H, Wang J, Zhu Y, Liu Y. 2014. Assessing consistency of five global land cover data sets in China. Remote Sens, 6: 8739–8759
Cheng Y, Yu L, Xu Y, Lu H, Cracknell A P, Kanniah K, Gong P. 2019. Mapping oil palm plantation expansion in Malaysia over the past decade (2007–2016) using ALOS-1/2 PALSAR-1/2 data. Int J Remote Sens, 40: 7389–7408
Cohen W, Healey S, Yang Z, Stehman S, Brewer C, Brooks E, Gorelick N, Huang C, Hughes M, Kennedy R, Loveland T, Moisen G, Schroeder T, Vogelmann J, Woodcock C, Yang L, Zhu Z. 2017. How similar are forest disturbance maps derived from different Landsat time series algorithms? Forests, 8: 98
Cotillon S E. 2017. West Africa land use and land cover time series. In: US Geological Survey. https://doi.org/10.3133/fs20173004
Dara A, Baumann M, Kuemmerle T, Pflugmacher D, Rabe A, Griffiths P, Hölzel N, Kamp J, Freitag M, Hostert P. 2018. Mapping the timing of cropland abandonment and recultivation in northern Kazakhstan using annual Landsat time series. Remote Sens Environ, 213: 49–60
Defourny P, Bontemps S, Lamarche C, Brockmann C, Boettcher M, Wevers J, Kirches G. 2017. Land Cover CCI: Product User Guide Version 2.0. http://maps.elie.ucl.ac.be/CCI/viewer/download/ESACCI-LC-PUG-v2.5.pdf
DeVries B, Decuyper M, Verbesselt J, Zeileis A, Herold M, Joseph S. 2015. Tracking disturbance-regrowth dynamics in tropical forests using structural change detection and Landsat time series. Remote Sens Environ, 169: 320–334
Ding C. 2003. Land policy reform in China: Assessment and prospects. Land Use Policy, 20: 109–120
Ding M, Chen Q, Xiao X, Xin L, Zhang G, Li L. 2016. Variation in cropping intensity in Northern China from 1982 to 2012 based on GIMMS-NDVI data. Sustainability, 8: 1123
Dong J, Xiao X, Kou W, Qin Y, Zhang G, Li L, Jin C, Zhou Y, Wang J, Biradar C, Liu J, Moore Iii B. 2015. Tracking the dynamics of paddy rice planting area in 1986–2010 through time series Landsat images and phenology-based algorithms. Remote Sens Environ, 160: 99–113
Dutrieux L P, Jakovac C C, Latifah S H, Kooistra L. 2016. Reconstructing land use history from Landsat time-series. Int J Appl Earth Observation Geoinf, 47: 112–124
Feng D, Yu L, Zhao Y, Cheng Y, Xu Y, Li C, Gong P. 2018. A multiple dataset approach for 30-m resolution land cover mapping: A case study of continental Africa. Int J Remote Sens, 39: 3926–3938
Feranec J, Soukup T, Hazeu G, Jaffrain G. 2016. European Landscape Dynamics: CORINE Land Cover Data. Boca Raton (FL): CRC Press
Forkel M, Carvalhais N, Verbesselt J, Mahecha M, Neigh C, Reichstein M. 2013. Trend change detection in NDVI time series: Effects of inter-annual variability and methodology. Remote Sens, 5: 2113–2144
Friedl M A, McIver D K, Hodges J C F, Zhang X Y, Muchoney D, Strahler A H, Woodcock C E, Gopal S, Schneider A, Cooper A, Baccini A, Gao F, Schaaf C. 2002. Global land cover mapping from MODIS: Algorithms and early results. Remote Sens Environ, 83: 287–302
Frolking S, Xiao X, Zhuang Y, Salas W, Li C. 1999. Agricultural land-use in China: A comparison of area estimates from ground-based census and satellite-borne remote sensing. GCTE/LUCC RESEARCH LETTER. Glob Ecol Biogeogr, 8: 407–416
Gao F, Anderson M C, Zhang X, Yang Z, Alfieri J G, Kustas W P, Mueller R, Johnson D M, Prueger J H. 2017. Toward mapping crop progress at field scales through fusion of Landsat and MODIS imagery. Remote Sens Environ, 188: 9–25
Gao F, Hilker T, Zhu X, Anderson M, Masek J, Wang P, Yang Y. 2015. Fusing Landsat and MODIS data for vegetation monitoring. IEEE Geosci Remote Sens Mag, 3: 47–60

Gong P, Li X, Zhang W. 2019. 40-year (1978–2017) human settlement changes in China reflected by impervious surfaces from satellite remote sensing. Sci Bull, 64: 756–763
Gong P, Niu Z G, Cheng X, Zhao K Y, Zhou D M, Guo J H, Liang L, Wang X F, Li D D, Huang H B, Wang Y, Wang K, Li W N, Wang X W, Ying Q, Yang Z Z, Ye Y F, Li Z, Zhuang D F, Chi Y B, Zhou H Z, Yan J. 2010. China's wetland change (1990–2000) determined by remote sensing. Sci China Earth Sci, 53: 1036–1042
Gong P, Wang J, Yu L, Zhao Y, Zhao Y, Liang L, Niu Z, Huang X, Fu H, Liu S, Li C, Li X, Fu W, Liu C, Xu Y, Wang X, Cheng Q, Hu L, Yao W, Zhang H, Zhu P, Zhao Z, Zhang H, Zheng Y, Ji L, Zhang Y, Chen H, Yan A, Guo J, Yu L, Wang L, Liu X, Shi T, Zhu M, Chen Y, Yang G, Tang P, Xu B, Giri C, Clinton N, Zhu Z, Chen J, Chen J. 2013. Finer resolution observation and monitoring of global land cover: First mapping results with Landsat TM and ETM+ data. Int J Remote Sens, 34: 2607–2654
Hansen M C, Loveland T R. 2012. A review of large area monitoring of land cover change using Landsat data. Remote Sens Environ, 122: 66–74
Hansen M C, Potapov P V, Moore R, Hancher M, Turubanova S A, Tyukavina A, Thau D, Stehman S V, Goetz S J, Loveland T R, Kommareddy A, Egorov A, Chini L, Justice C O, Townshend J R G. 2013. High-resolution global maps of 21st-century forest cover change. Science, 342: 850–853
He Y, Lee E, Warner T A. 2017. A time series of annual land use and land cover maps of China from 1982 to 2013 generated using AVHRR GIMMS NDVI3g data. Remote Sens Environ, 199: 201–217
Holben B N. 1986. Characteristics of maximum-value composite images from temporal AVHRR data. Int J Remote Sens, 7: 1417–1434
Hu L Y, Chen Y L, Xu Y, Zhao Y Y, Yu L, Wang J, Gong P. 2014. A 30 meter land cover mapping of China with an efficient clustering algorithm CBEST. Sci China Earth Sci, 57: 2293–2304
Hu X, Lu L, Li X, Wang J, Guo M. 2015. Land use/cover change in the middle reaches of the Heihe River Basin over 2000–2011 and its implications for sustainable water resource management. PLoS One, 10: e0128960
Huang C, Goward S N, Masek J G, Thomas N, Zhu Z, Vogelmann J E. 2010. An automated approach for reconstructing recent forest disturbance history using dense Landsat time series stacks. Remote Sens Environ, 114: 183–198
Jin S, Yang L, Zhu Z, Homer C. 2017. A land cover change detection and classification protocol for updating Alaska NLCD 2001 to 2011. Remote Sens Environ, 195: 44–55
de Jong R, Verbesselt J, Zeileis A, Schaepman M. 2013. Shifts in global vegetation activity trends. Remote Sens, 5: 1117–1133
de Jong R, Verbesselt J, Schaepman M E, Bruin S. 2012. Trend changes in global greening and browning: Contribution of short-term trends to longer-term change. Glob Change Biol, 18: 642–655
Kennedy R E, Yang Z, Cohen W B. 2010. Detecting trends in forest disturbance and recovery using yearly Landsat time series: 1. LandTrendr —Temporal segmentation algorithms. Remote Sens Environ, 114: 2897–2910
Kwan C, Budavari B, Gao F, Zhu X. 2018. A hybrid color mapping approach to fusing MODIS and Landsat images for forward prediction. Remote Sens, 10: 520
Li C, Gong P, Wang J, Zhu Z, Biging G S, Yuan C, Hu T, Zhang H, Wang Q, Li X, Liu X, Xu Y, Guo J, Liu C, Hackman K O, Zhang M, Cheng Y, Yu L, Yang J, Huang H, Clinton N. 2017. The first all-season sample set for mapping global land cover with Landsat-8 data. Sci Bull, 62: 508–515
Li X, Gong P, Liang L. 2015. A 30-year (1984–2013) record of annual urban dynamics of Beijing City derived from Landsat data. Remote Sens Environ, 166: 78–90
Li X, Yu L, Xu Y, Yang J, Gong P. 2016. Ten years after Hurricane Katrina: Monitoring recovery in New Orleans and the surrounding areas using remote sensing. Sci Bull, 61: 1460–1470
Lin G C S, Ho S P S. 2003. China's land resources and land-use change: Insights from the 1996 land survey. Land Use Policy, 20: 87–107
Liu X, Huang J, Huang J, Li C, Ding L. 2019. Impact of anthropogenic activities on global land oxygen flux. Earth Syst Sci Data Discuss, doi: 0.5194/essd-2019-36
Liu J, Kuang W, Zhang Z, Xu X, Qin Y, Ning J, Zhou W, Zhang S, Li R, Yan C, Wu S, Shi X, Jiang N, Yu D, Pan X, Chi W. 2014. Spatiotemporal characteristics, patterns, and causes of land-use changes in China since the late 1980s. J Geogr Sci, 24: 195–210
Liu J, Liu M, Tian H, Zhuang D, Zhang Z, Zhang W, Tang X, Deng X. 2005. Spatial and temporal patterns of China's cropland during 1990–2000: An analysis based on Landsat TM data. Remote Sens Environ, 98: 442–456
Liu J, Liu M, Zhuang D, Zhang Z, Deng X. 2003. Study on spatial pattern of land-use change in China during 1995–2000. Sci China Ser D-Earth Sci, 46: 373–384
Lu M, Wu W B, Zhang L, Liao A P, Peng S, Tang H J. 2016. A comparative analysis of five global cropland datasets in China. Sci China Earth Sci, 59: 2307–2317
Lunetta R S, Knight J F, Ediriwickrema J, Lyon J G, Worthy L D. 2006. Land-cover change detection using multi-temporal MODIS NDVI data. Remote Sens Environ, 105: 142–154
Ngcofe L, Thompson M. 2015. The status of land cover mapping in South Africa: 1994–2015. In: EE Publishers. https://www.ee.co.za/article/status-land-cover-mapping-south-africa-1994-2015.html
Ning J, Liu J, Kuang W, Xu X, Zhang S, Yan C, Li R, Wu S, Hu Y, Du G, Chi W, Pan T, Ning J. 2018. Spatiotemporal patterns and characteristics of land-use change in China during 2010–2015. J Geogr Sci, 28: 547–562
Pekel J F, Cottam A, Gorelick N, Belward A S. 2016. High-resolution mapping of global surface water and its long-term changes. Nature, 540: 418–422
Permatasari P A, Fatikhunnada A, Liyantono A, Setiawan Y, Syartinilia Y, Nurdiana A. 2016. Analysis of agricultural land use changes in jombang regency, East Java, Indonesia Using BFAST method. Procedia Environ Sci, 33: 27–35
Quarfeld J, di Mauro B, Colombo R, Verbesselt J. 2016. Exploring fire dynamics with BFAST approach: Case studies in Sardinia, Italy. In: EGU General Assembly Conference Abstracts
Schneider A, Mertes C M. 2014. Expansion and growth in Chinese cities, 1978–2010. Environ Res Lett, 9: 024008
Smil V. 1999. China's agricultural land. China Q, 158: 414–429
Song X P, Hansen M C, Stehman S V, Potapov P V, Tyukavina A, Vermote E F, Townshend J R. 2018. Global land change from 1982 to 2016. Nature, 560: 639–643
Verbesselt J, Hyndman R, Newnham G, Culvenor D. 2010a. Detecting trend and seasonal changes in satellite image time series. Remote Sens Environ, 114: 106–115
Verbesselt J, Hyndman R, Zeileis A, Culvenor D. 2010b. Phenological change detection while accounting for abrupt and gradual trends in satellite image time series. Remote Sens Environ, 114: 2970–2980
Verbesselt J, Zeileis A, Herold M. 2012. Near real-time disturbance detection using satellite image time series. Remote Sens Environ, 123: 98–108
Waldner F, Canto G S, Defourny P. 2015. Automated annual cropland mapping using knowledge-based temporal features. ISPRS J Photogrammetry Remote Sens, 110: 1–13
Watts L M, Laffan S W. 2014. Effectiveness of the BFAST algorithm for detecting vegetation response patterns in a semi-arid region. Remote Sens Environ, 154: 234–245
Xu Y, Yu L, Peng D, Cai X, Cheng Y, Zhao J, Zhao Y, Feng D, Hackman K, Huang X, Lu H, Yu C, Gong P. 2018a. Exploring the temporal density of Landsat observations for cropland mapping: Experiments from Egypt, Ethiopia, and South Africa. Int J Remote Sens, 39: 7328–7349
Xu Y, Yu L, Zhao F R, Cai X, Zhao J, Lu H, Gong P. 2018b. Tracking annual cropland changes from 1984 to 2016 using time-series Landsat images with a change-detection and post-classification approach: Ex-

periments from three sites in Africa. Remote Sens Environ, 218: 13–31
Xu Y, Yu L, Zhao Y, Feng D, Cheng Y, Cai X, Gong P. 2017. Monitoring cropland changes along the Nile River in Egypt over past three decades (1984–2015) using remote sensing. Int J Remote Sens, 38: 4459–4480
Yin H, Pflugmacher D, Li A, Li Z, Hostert P. 2018. Land use and land cover change in Inner Mongolia—Understanding the effects of China's re-vegetation programs. Remote Sens Environ, 204: 918–930
Yu L, Shi Y, Gong P. 2015. Land cover mapping and data availability in critical terrestrial ecoregions: A global perspective with Landsat thematic mapper and enhanced thematic mapper plus data. Biol Conservation, 190: 34–42
Yu L, Wang J, Clinton N, Xin Q, Zhong L, Chen Y, Gong P. 2013. FROM-GC: 30 m global cropland extent derived through multisource data integration. Int J Digital Earth, 6: 521–533
Yu L, Wang J, Li X C, Li C C, Zhao Y Y, Gong P. 2014. A multi-resolution global land cover dataset through multisource data aggregation. Sci China Earth Sci, 57: 2317–2329
Zeileis A. 2005. A unified approach to structural change tests based on ML scores, F statistics, and OLS residuals. Econ Rev, 24: 445–466
Zhang L, Weng Q, Shao Z. 2017. An evaluation of monthly impervious surface dynamics by fusing Landsat and MODIS time series in the Pearl River Delta, China, from 2000 to 2015. Remote Sens Environ, 201: 99–114
Zhao F, Meng R, Huang C, Zhao M, Zhao F, Gong P, Yu L, Zhu Z. 2016. Long-term post-disturbance forest recovery in the greater yellowstone ecosystem analyzed using Langsat time series stack. Remote Sens, 8: 898
Zhao Y, Feng D, Yu L, Cheng Y, Zhang M, Liu X, Xu Y, Fang L, Zhu Z, Gong P. 2019. Long-term land cover dynamics (1986–2016) of Northeast China derived from a multi-temporal Langsat archive. Remote Sens, 11: 599
Zhao Y, Gong P, Yu L, Hu L, Li X, Li C, Zhang H, Zheng Y, Wang J, Zhao Y, Cheng Q, Liu C, Liu S, Wang X. 2014. Towards a common validation sample set for global land-cover mapping. Int J Remote Sens, 35: 4795–4814
Zhong L, Gong P, Biging G S. 2014. Efficient corn and soybean mapping with temporal extendability: A multi-year experiment using Landsat imagery. Remote Sens Environ, 140: 1–13
Zhou W, Yang H, Huang L, Chen C, Lin X, Hu Z, Li J. 2017. Grassland degradation remote sensing monitoring and driving factors quantitative assessment in China from 1982 to 2010. Ecol Indicat, 83: 303–313
Zhu Z, Woodcock C E. 2014. Continuous change detection and classification of land cover using all available Landsat data. Remote Sens Environ, 144: 152–171

(Responsible editor: Jiancheng SHI)